Atmospheric Environment 191 (2018) 463–477

Contents lists available at ScienceDirect

Atmospheric Environment

journal homepage: www.elsevier.com/locate/atmosenv

Multi-scale correlations between air quality and meteorology in the Guangdong – Hong Kong – Macau Greater Bay Area of China during 2015–2017

Xingqin Fang*, Qi Fan, Haowen Li, Zhiheng Liao, Jielan Xie, Shaojia Fan**

School of the Atmospheric Sciences/Guangdong Province Key Laboratory for Climate Change and Natural Disaster Studies, Sun Yat-sen University, Guangzhou, 510275, China

ARTICLE INFO

Keywords:
Multi-scale correlations
Air quality
Air pollution meteorology
Particulate matter
Ozone
Guangdong – Hong Kong – Macau Greater Bay area

ABSTRACT

A multi-scale correlation analysis method is introduced and a combined analysis of multi-scale correlations between air quality and meteorology in Guangdong-Hong Kong-Macao Greater Bay Area (GHMGBA) of China is performed using 3-yr daily series of particulate matter (PM) fractions and O_3 observations and collocated meteorological reanalysis data during 2015–2017. PM and O_3 have significant seasonal oscillation and oscillations of 2–3 days, 5–7 days, quasi two weeks, and 20–30 days, which are typical periods in east-west wind (U), north-south wind (V), wind speed (WS), temperature (T), relative humidity (RH), 925-hPa specific humidity (Q), and surface air pressure (SP), although different types of meteorological parameters have different significant periods. In GHMGBA, the East Asian Monsoon has different significant impacts on PM and O_3. The relationships of air quality with meteorology on higher frequency modes are usually very different from those on lower frequency modes since different mechanisms make effects. Correlation details may also differ on different synoptic scales. Especially, PM has consistent significant negative correlations with V, T, RH, and Q on seasonal oscillation but has large positive (negative) correlations with V, T, and Q (WS and SP) on oscillations of 2–3 days, 5–7 days, and quasi two weeks in winter half year. The latter synoptic correlations reflect the impact of the typical quasi-stationary front and cold front activities on PM, which usually includes two sequential asymmetric processes: a long no-precipitation stagnation period when ventilation, dilution, and hygroscopic growth make effects; and a short precipitation period when ventilation, dilution, and wet deposition make effects. In a word, local synoptic scales correlations cannot be directly extended to estimate the response of air quality to climate change projections.

1. Introduction

The Guangdong – Hong Kong – Macao Greater Bay Area (GHMGBA, Fig. 1) of China includes nine cities of Guangdong province – Guangzhou, Shenzhen, Zhuhai, Foshan, Huizhou, Dongguan, Zhongshan, Jiangmen and Zhaoqing – as well as the Hong Kong SAR and the Macao SAR. It covers an area of 56,000 square kilometers, and has 68 million permanent residents. This area has been observed the most rapid economic development in China during the last two decades. In GHMGBA, complex air pollution issues, represented by high levels of urban and regional fine particulate matter (PM) and Ozone (O_3) concentrations associated with photochemical reactions, are getting more and more concern (Wu et al., 2014a). It has been a consensus to pursue sustainable economic development and avoid fatal air pollution events that happened decades ago during the old style of urbanization and industrialization. Many cooperative efforts from the local governments have been made to monitor air quality and control air pollution in this area.

Emissions of primary pollutants, ambient natural environments such as topography and sea-land contrast, and meteorological conditions are all important impact factors of air quality. In general, pollutant sources and ambient natural environments do not change much during a short period; however, the atmospheric circulations have complicated multi-scale coherent structures and variations (Fang and Kuo, 2015). Therefore, the air quality at any specific location has very complicated variations that could not be explained only by sources and meteorological conditions play an import role (Galindo et al., 2010; Yadav et al., 2014; Zhang et al., 2016; Zhou et al., 2013). Complicated climate variability

* Corresponding author.
** Corresponding author.
E-mail addresses: fangxq7@mail.sysu.edu.cn (X. Fang), eesfsj@mail.sysu.edu.cn (S. Fan).

https://doi.org/10.1016/j.atmosenv.2018.08.018
Received 15 April 2018; Received in revised form 7 August 2018; Accepted 9 August 2018
Available online 11 August 2018
1352-2310/ © 2018 Elsevier Ltd. All rights reserved.

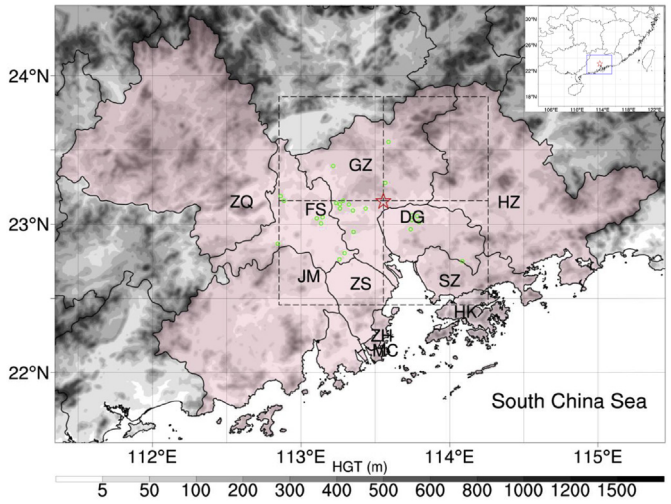

Fig. 1. Topography map of the Guangdong – Hong Kong – Macao Greater Bay Area (GHMGBA, the pinked area) and its surroundings (see the blue box in the superimposed administrative map for reference). The GHMGBA includes 11 cities: Guangzhou (GZ), Zhaoqing (ZQ), Foshan (FS), Dongguan (DG), Huizhou (HZ), Jiangmen (JM), Zhongshan (ZS), Shenzhen (SZ), Zhuhai (ZH), Hong Kong (HK), and Macao (MC). The four dashed boxes centered at (22.807°N, 113.203°E), (23.509°N, 113.203°E), (22.807°N, 113.906°E), and (23.509°N, 113.906°E), respectively, show the closest model grids where the ERA-Interim reanalysis data (in a resolution of 0.75° × 0.75°) are extracted as the collocated meteorological data for the air quality data at cities FS, GZ, DG, and HZ, respectively; and they are denoted as ECF, ECG, ECD, and ECH, respectively. The point (23.158°N, 113.555°E) marked by a red star is the common vertex of the four model grids and for convenience it is selected as the representative point to anchor the geographical location for GHMGBA in the larger scale administrative map. The green circles are the loci of observation stations.

and diverse aerosol feedbacks (Jacobson, 2001; Rosenfeld et al., 2014) make it uneasy to see instant air quality improvement from emission control. In order to respond to public health concern, it is necessary to interpret air quality variabilities from meteorological aspect. The investigation of relationships between air quality and meteorological situations also helps to build up air quality forecast capacity and contributes to coordinated air pollution control.

One approach for projecting the influence of climate change on air quality is using the general circulation model (GCM) coupled with chemical transport model (CTM). But this way is expensive and there are many uncertainties. An alternative approach is using statistical models. The observational air quality-meteorology relationships are not only essential for the statistical approach but also useful for testing parameters in the GCM-CTM approach. Many studies on air quality-meteorology correlations have been performed on various specific scales, but based on our knowledge, this paper is the first attempt to address the combined multi-scale air quality-meteorology correlations.

Some previous studies intended to test and calibrate the chemical transport model or extend the synoptic scale correlation to simulate or estimate the response of aerosol to climate change (Dawson et al., 2007; Tai et al., 2010); while others tried to identify significant meteorological impact factors on air quality, in terms of either individual parameters or certain synoptic patterns, to build up efficient day-to-day air quality statistic forecasts. The meteorological influences vary significantly across seasons and locations (Zhang et al., 2015). As indicated in Li et al. (2017), the relationship of PM_{10} and $PM_{2.5}$ with meteorology is complicated. They found that high air temperature favors the transformation of secondary PM through photochemical processes in summer, but also results in efficient vertical dispersion of pollutants in autumn and winter. Large relative humidity usually causes increases in PM concentrations due to the hygroscopic effect of aerosols, but not for PM_{10} in spring and summer, mainly due to the suppression of dust emissions under wet air conditions in spring and the effects of wet scavenging under high summer rainfall. Recently, Leung et al. (2017) suggested that the apparent correlations with individual meteorological variables may arise from common association with synoptic systems and recommended a process-based modeling. Zhang et al. (2012) investigated the air quality characteristics of different circulation patterns derived from surface level pressure over a region around Beijing, China and suggested that the circulation pattern types are the primary drivers of day-to-day variations of air quality. Liao et al. (2018) examined the regulating effects of different atmospheric boundary layer (ABL) types on Beijing's air quality and otherwise suggested that the ABL types are the primary drivers of day-to-day variations in Beijing's air quality. Some studies (Fan et al., 2008, 2011; Wu et al., 2013, 2014b) also found that the ABL characteristics are important for identifying the air pollution problem in GHMGBA. Recently, Li et al. (2018) examined the combined effects of the recirculation index and stable energy on air quality at Foshan for two typical episodes.

Actually, either the horizontal circulation or the vertical structure is a coherent part of the whole atmospheric system. It is a good idea to investigate air quality-meteorology correlations with a coherent multi-scale continuum of atmosphere in mind. A combined analysis of air quality-meteorology correlations not only involves multivariate correlations with meteorology on various timescales, but also considers behaviors of different coexisting pollutants as well as air quality diversity among neighboring cities. It is expected that based on the general emission information, some details on physical and chemical mechanisms behind air quality variations might be derived from a combined analysis.

For cities in GHMGBA of China, Ji et al. (2006) applied wavelet analysis to the air quality time series and found that all of the investigated air quality concentrations exhibit significant annual cycles and oscillations of 5–7 days, 10–20 days, and 30–60 days. However, they did not perform multi-scale correlation analysis. In this paper, we attempt to study the multi-scale correlations between air quality and meteorology in GHMGBA using daily mean time series of air quality observations of PM_{10}, $PM_{2.5}$, and O_3 and relevant meteorological reanalysis data during 2015–2017. The Ensemble Empirical Mode Decomposition (EEMD) method (Wu et al., 2016; Wu and Huang, 2009) is applied to get the multi-scale intrinsic mode functions (IMFs) of both air quality and meteorology datasets. By applying the correlation analysis on decomposed modes, it is convenient to separate correlations on different scales without any other subjective filtering or smoothing. The scale separation also benefits for the investigation of correlation mechanisms between air quality and meteorology on individual scale. The paper is organized as follows. Section 2 introduces the data and method. Section 3 performs multi-scale correlation analysis of air quality and meteorology and interprets correlation mechanisms scale by scale. Finally, Section 4 gives conclusions.

2. Data and method

2.1. Data

In this paper, a particular emphasis is paid on a region FGD in GHMGBA which is composed of three neighboring cities Foshan (FS), Guangzhou (GZ), and Dongguan (DG). The air quality variables studied include PM_{10}, $PM_{2.5}$, and O_3. The collocated meteorological parameters investigated include surface air pressure (SP), 10-m east-west wind (U), 10-m north-south wind (V), 10-m wind speed (WS), 2-m temperature (T), 2-m relative humidity (RH), and 925-hPa specific humidity (Q).

Daily mean air quality observations at FS, GZ, and DG during 2015–2017 from a research website (https://www.zq12369.com) are used for time series analysis. The percentage of missing data is less than 1% and they are all rescued using a simple linear interpolation method. The small scale air quality variations within a city are omitted and the

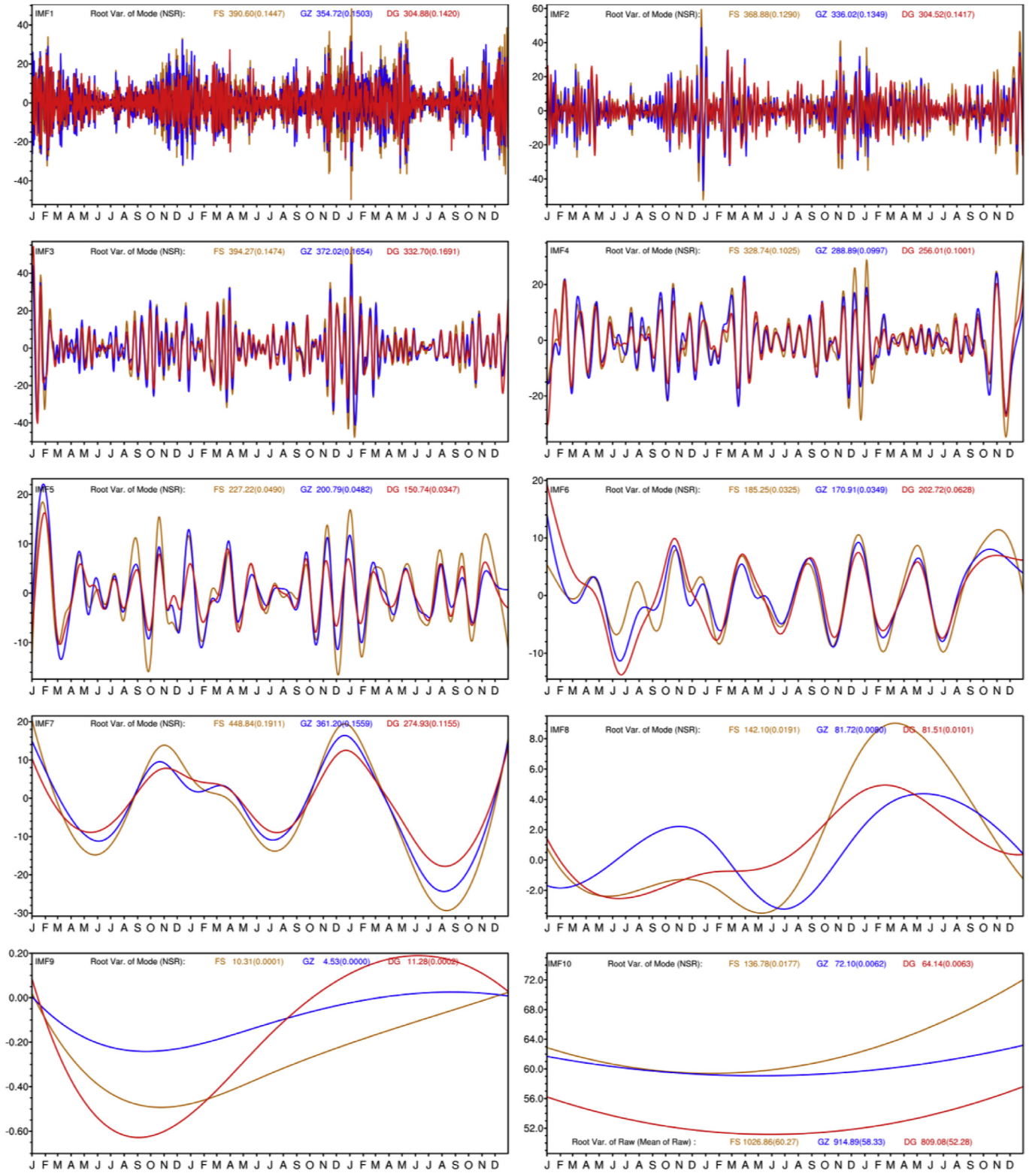

Fig. 2. Daily time series of EEMD intrinsic mode functions (IMFs) (unit: μg/m^3) of PM_{10} during 2015–2017 at FS, GZ, and DG. The corresponding square root of variance (unit: μg/m^3) and NSR_{IMF} are listed at top of plots for IMFs 1–10. The square root of variance (unit: μg/m^3) and mean (unit: μg/m^3) for raw time series are listed at bottom of plot for IMF10.

mean value derived from the monitoring stations (featured as traffic, urban, industry, background, etc.) carefully laid by environment monitoring authorities is taken as the representative air quality value for a citywide area. The loci of observation stations are shown in Fig. 1. There are generally about 5–10 stations scattered within a city. Since the observation stations are not evenly distributed (with more stations located in the urban areas), the city mean air quality may have different representativeness at different cities. But the representative errors and differences should not be large enough to affect the results and conclusions of the daily mean time series analysis in this paper. The

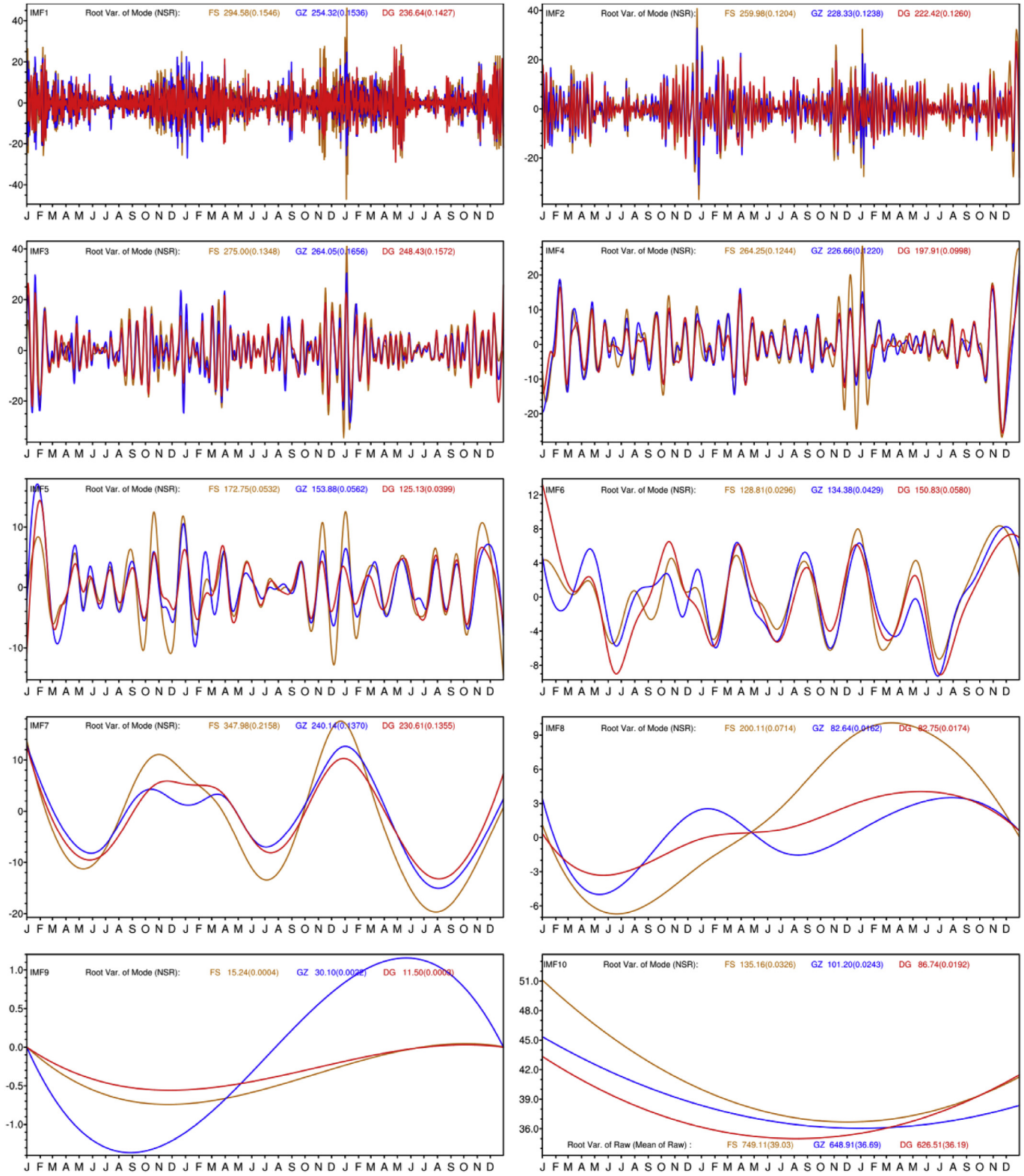

Fig. 3. The same as Fig. 2 but for $PM_{2.5}$.

meteorological data used in this study are from the European Center for Medium Range Weather Forecast (ECMWF) Re-Analysis (ERA) (Dee et al., 2011). The ERA-Interim data structured in a resolution of 0.75° × 0.75° are available at a website (https://rda.ucar.edu/datasets/ds627.0/). Daily ERA-Interim data at 0600 UTC (i.e., 1400 LST) on model grids ECF, ECG, and ECD (see Fig. 1) are selected to represent the collocated meteorological data for air quality at FS, GZ, and DG, respectively.

Since the cities in GHMGBA are influenced by the East Asian Monsoon (EAM) and have obvious alternating wet and dry season of precipitation, different sampling periods of full year (FUL), winter half year (i.e., dry season) (WIN, from November to April), and summer half year (i.e., wet season) (SUM, from May to October) are considered.

2.2. Methods

The idea of empirical mode decomposition (EMD) originated from the Hilbert – Huang transform (Huang et al., 1996). This decomposition method is adaptive to locality since it utilizes local minima and maxima to extract the IMFs from raw data. Sequentially, N oscillatory IMFs from higher to lower frequency are extracted and the residual is a non-oscillatory trend mode that consists of the background state and a trend. Each IMF represents an oscillation on a band of comparable scales, and the frequencies or periods can be estimated by the numbers of local minima and maxima. The EMD method is useful for data analysis and has been widely applied in many fields including meteorology, but it has never been used for multi-scale correlations analysis of air quality data. Issues of mode mixing or frequency aliasing in EMD sometimes present, where signals of disparate scales are mixed in one mode or a signal of similar scales presents in different modes. As indicated in Huang et al. (1998), these issues result from signal intermittency and could lead to indistinct physical meaning of individual modes. The EEMD introduced by Wu and Huang (2009) is a noise assisted EMD, where the EMD is performed on a noise-added ensemble of datasets. The EEMD method reduces the chance of frequency aliasing and is suitable for processing series that are non-stationary and non-linear. The newest open version of NCAR (National Center for Atmospheric Research) Command Language (NCL, http://www.ncl.ucar.edu) v6.4.0 provides the EEMD code.

A multi-scale correlation analysis is introduced in this paper with correlation coefficients calculated using the corresponding daily time series of decomposed IMFs. For a comparison, the traditional correlation analysis is also performed using daily time series of raw datasets.

Resembling the noise-to-signal ratio (NSR) concept in Fang and Kuo (2015), we quantify the relative importance of IMFs with NSR_{IMF} defined as

$$NSR_{IMF} = \frac{\sum_{it=1}^{M} X_{IMF}^2(it)}{\sum_{it=1}^{M} [X(it) - \overline{X}]^2}, \quad (1)$$

where $X(it)$ is a raw time series with $it = 1,2...M$, $\overline{X}$ is the temporal mean, $X_{IMF}(it)$ is a decomposed IMF time series with $it = 1,2...M$, and M is the total length of time series (either monthly mean or daily mean series).

By definition, the NSR_{IMF} values of different modes for different variables at different locations for different sampling periods are all comparable. In the following analysis, the oscillation of an individual IMF is thought to be significant if the corresponding NSR_{IMF} value is larger than a criterion $\varphi^{-6} \cong 0.0557$, where $\varphi = (1 + \sqrt{5})/2$.

3. Multi-scale correlation analysis of air quality and meteorology

3.1. Decomposed time series of air quality and meteorology in FGD

Nine oscillatory IMFs (noted as IMFs 1–9) and one trend mode (noted as IMF10) are extracted for each daily dataset of air quality variables and meteorological parameters in FGD using the EEMD method. Figs. 2–4 show daily series of EEMD IMFs of PM_{10}, $PM_{2.5}$, and O_3, respectively, during 2015–2017. From the numbers of local maxima and minima, the periods of oscillations can be estimated as follows. IMFs 1–4 represent for sub-monthly oscillations of 2–3 days, 5–7 days, quasi two weeks, and 20–30 days, respectively. IMFs 5 and 6 are for inter-seasonal oscillations of 40–60 days and 80–90 days, respectively. IMF7 is for the seasonal oscillation. IMFs 8 and 9 are for inter-annual fluctuations resolved by available data samples. IMF10 includes the background state and a trend. As a good example, the zoomed segmental series of IMFs 1–7 of $PM_{2.5}$ from 1 October 2016 to 31 March 2017 in Fig. 5a depict that the coherent multi-scale developments on modes IMFs 1–7 produce an extreme $PM_{2.5}$ air pollution episode at FS in January 2017. To present the higher frequencies in more details, Fig. 5b shows a zoomed-in segmental series of IMFs 1 and 2 of $PM_{2.5}$ from 1 December 2016 to 1 February 2017. Fig. 6 shows daily time series of EEMD IMFs of U, V, WS, RH, T, Q, and SP during 2015–2017.

Following Eq. (1), the NSR_{IMF} values of modes IMFs 1–10 of each dataset are calculated (see Table 1 for values of IMFs 1–7). It is found that the air quality in FGD has very significant seasonal oscillation, which suggests the important impact of EAM on air quality. All PM fractions and O_3 have significant common sub-monthly oscillation periods of 2–3 days, 5–7 days, quasi two weeks, and 20–30 days although the significance is variable and has inter-city diversity. O_3 also has significant inter-seasonal low frequency oscillations of about 40–60 days and 80–90 days in winter half year. In addition, air quality in FGD has obvious inter-annual anomalies during 2015–2017. It is also found that V, U, SP, T, Q, and RH in FGD have significant seasonal oscillations which reflect the EAM signals; but WS do not have significant seasonal oscillation. U, V, WS, and RH in FGD have significant oscillations of 2–3 days, 5–7 days, and quasi two weeks. U and RH also have significant 20–30 days' oscillations. T (except for T at ECD) has significant quasi two weeks' oscillation. RH and V (except for V at ECG) have significant 40–60 days' oscillations. T, Q, and SP in FGD are generally much more stable than other parameters on higher frequency modes and their seasonal oscillations are extremely significant. The significance of oscillations also has obvious seasonal dependence.

It should be noted that the amplitude evolution of 5–7 days' period in Fig. 5b does not present too much “weekend-weekday” difference. That is, the so-called “weekend effect” is not obvious in the studied air quality time series. One reason for this fact is that the city-wide averaging has removed the possible “weekend effect” associated with small scale phase-locked emissions. And besides, day-to-day changes of emissions are general very small. Actually, the 5–7 days' period is a typical meteorological period which is usually controlled by the synoptic scale Rossby waves. As will be shown in the following text, the impacts from meteorological conditions on the 5–7 days' oscillation of city mean daily air quality are very significant. Therefore, compared with the impacts from meteorological conditions, the impacts from changes of emissions on changes of city mean daily air quality are small.

3.2. Multi-scale correlations versus whole-scale correlations

The FUL, WIN, and SUM sampling multi-scale correlation coefficients on modes IMFs 1–7 at FS are listed in Tables 2–4 for correlations with PM_{10}, $PM_{2.5}$, and O_3 respectively. The corresponding multi-scale correlation coefficients at GZ and DG are omitted for simplicity. The correlations on modes IMFs 8–10 are not considered here since the oscillation energies on these modes are very small. The FUL, WIN, and SUM sampling whole-scale correlation coefficients of air quality variables including PM_{10}, O_3, and $PM_{2.5}$ and various meteorological parameters including U, V, WS, T, RH, Q, and SP calculated using the daily raw time series during 2015–2017 at FS, GZ, and DG are listed in Table 5.

As shown in Tables 2–4, air quality-meteorology correlation coefficients on different modes are usually different, and the significance of correlations on some modes has large seasonal dependence. The comparison with results in Table 5 indicates that the apparent whole scale correlation coefficients can reflect real correlations well if the correlations on various modes are consistent, like for correlations with WS; but cannot reflect real correlation details if the correlations on various frequency bands are very different even contrary, like correlations with T or Q. For example, as shown in the FUL sampling results in Tables 2–4, PM_{10} and $PM_{2.5}$ have good positive correlations with V on higher frequency oscillations but good negative correlations on 80–90 days' oscillation and seasonal oscillation; $PM_{2.5}$ has good positive correlations with T on sub-monthly oscillations but good negative correlation on 80–90 days' oscillation and seasonal oscillation; $PM_{2.5}$ has good positive correlation with Q on 2–3 days' oscillation but good negative

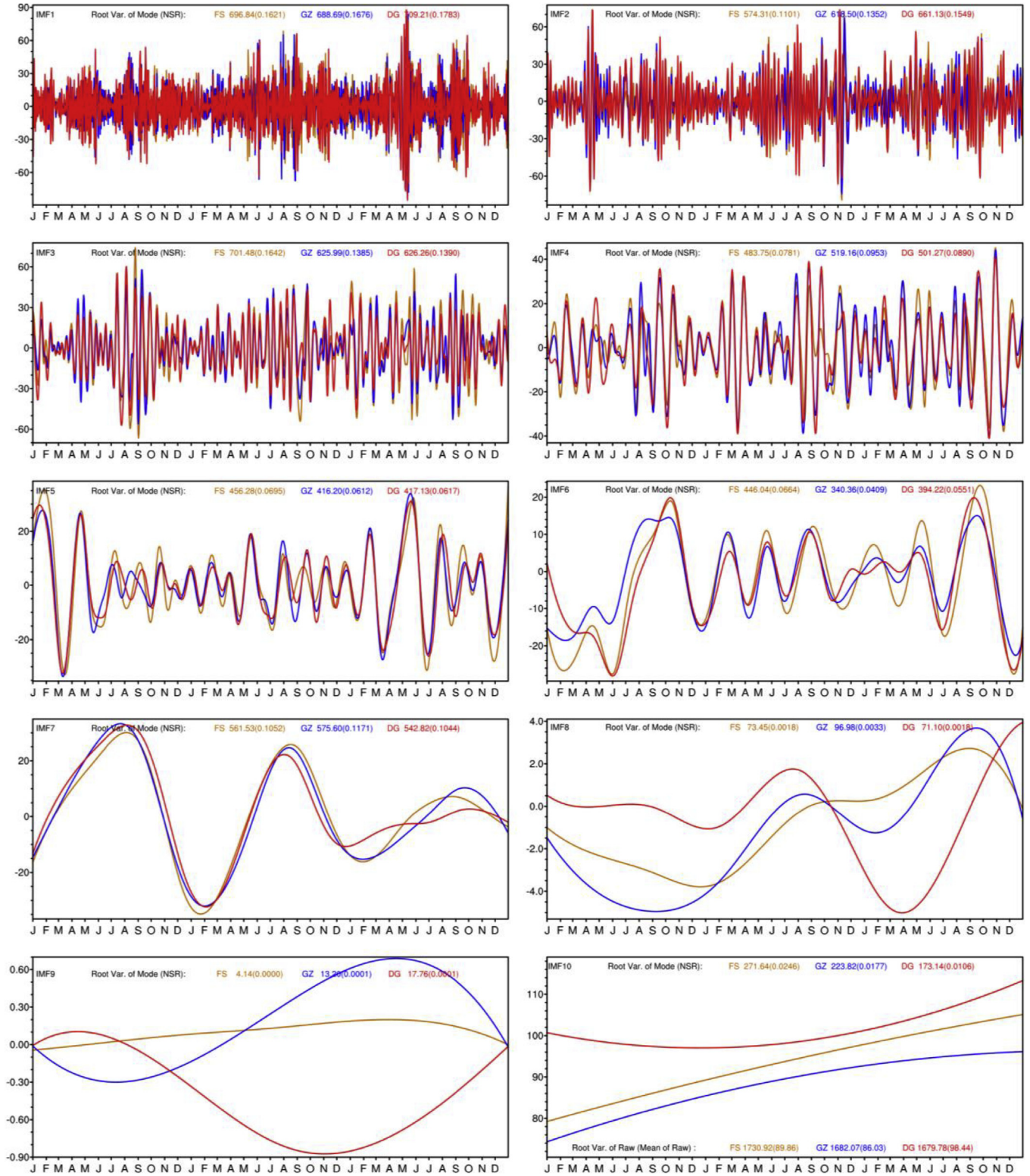

Fig. 4. The same as Fig. 2 but for O_3.

correlations on 20–30 days' oscillation and inter-seasonal oscillations; O_3 has good negative correlations with Q on oscillations of quasi two weeks, 20–30 days, and 40–60 days but good positive correlations on 80–90 days' oscillation and seasonal oscillation. Obviously, it is impossible to separate synoptic scale correlations from lower frequency correlations simply with the whole-scale correlation analysis. In order to focus on synoptic scales, Tai et al. (2010) tried to use the deseasonalized and detrended meteorological data for the correlation and regression analysis by subtracting the 30-day moving averages from raw data. However, they still could not separate correlations on different synoptic scales. By applying the correlation analysis on decomposed modes, we can separate correlations on different scales without any other filtering or smoothing. In addition, the coherent multi-scale correlation analysis makes it possible to investigate

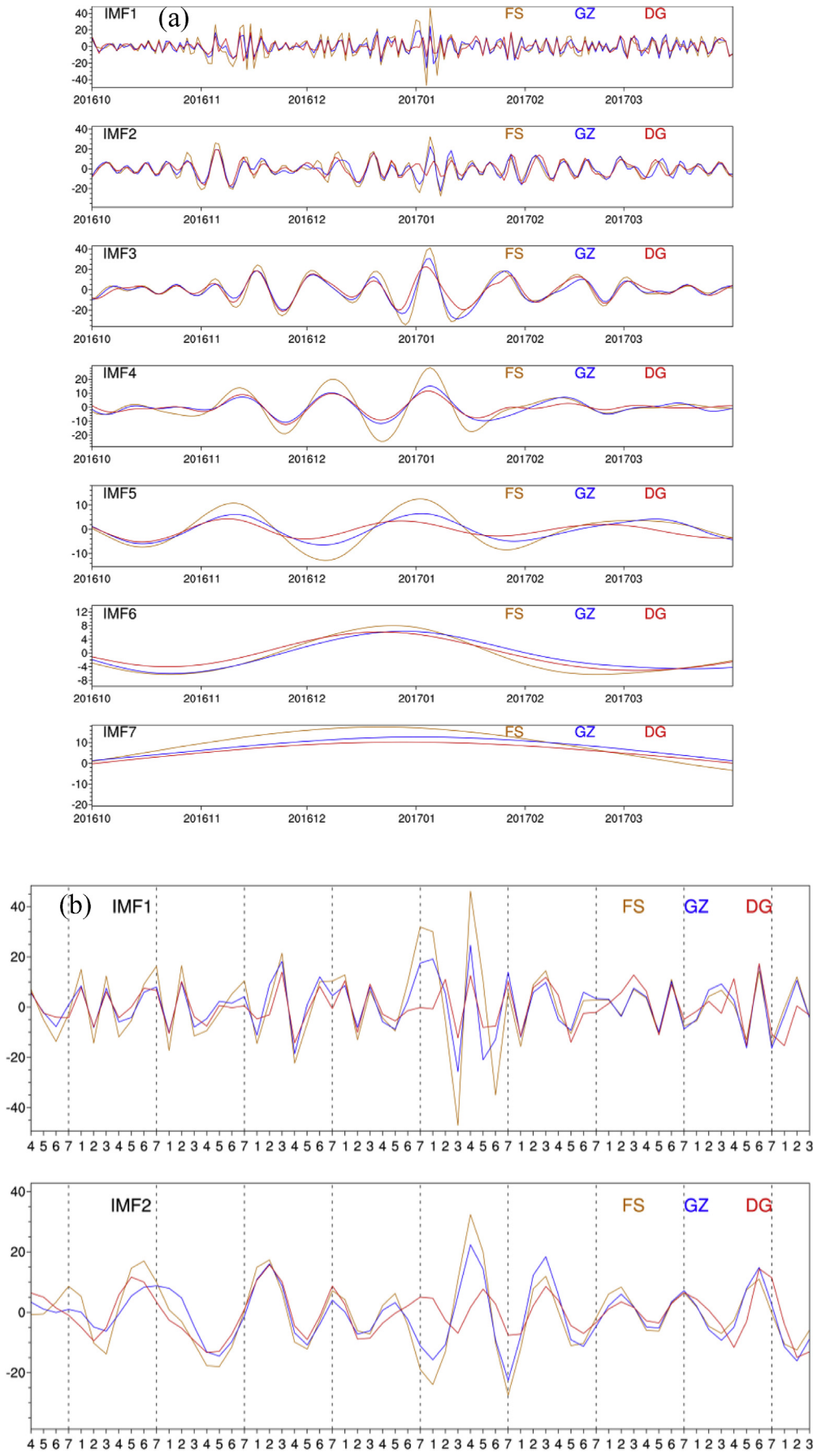

Fig. 5. Highlighted daily time series of IMFs of $PM_{2.5}$ (unit: μg/m^3) at FS, GZ, and DG: (a) IMFs 1–7 from October 2016 to March 2017; (b) IMFs 1 and 2 from 1 December 1, 2016 to 1 February 2017. The X axis in (b) is labelled in weekly cycle with "1" represents "Monday" and so on.

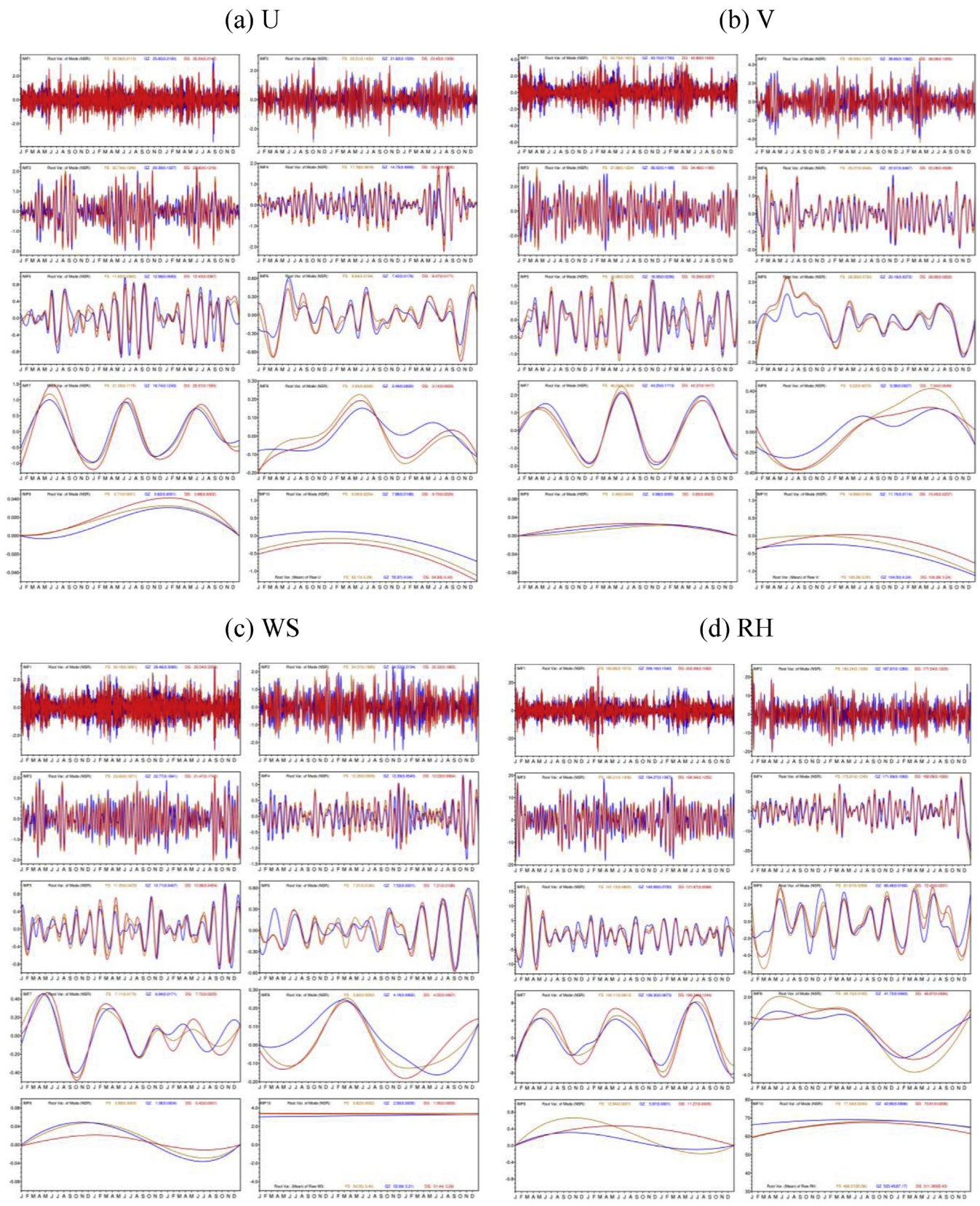

Fig. 6. Daily time series of EEMD intrinsic mode functions (IMFs) of (a) U (unit: m/s), (b) V (unit: m/s), (c) WS (unit: m/s), (d) RH (unit: %), (e) T (unit: °C), (f) Q (unit: mg/kg^3), and (g) SP (unit: hPa) during 2015–2017 at model grids ECF, ECG, and ECD representing for FS, GZ, and DG, respectively. The corresponding square root of variance and NSR_{IMF} are listed at top of plots for IMFs 1–10. The square root of variance and mean for raw time series are listed at bottom of plot for IMF10.

(e) T (f) Q

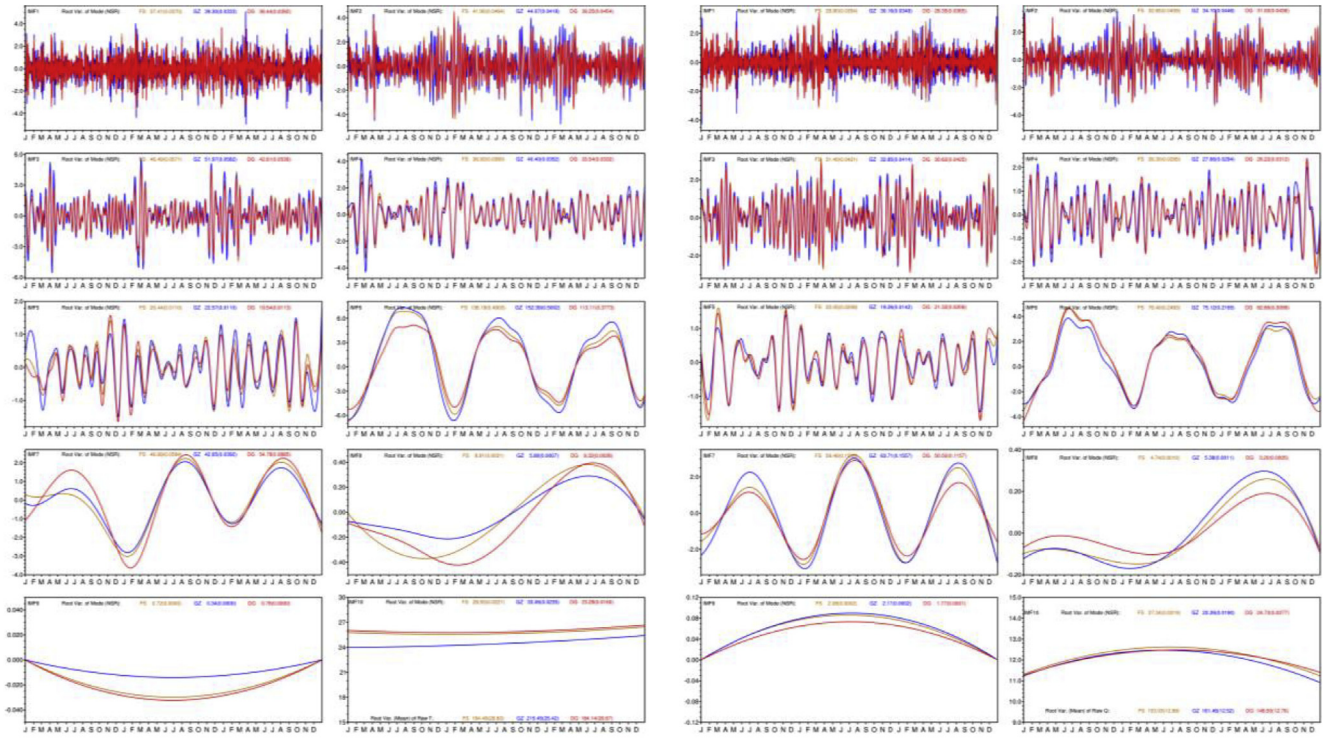

(g) SP

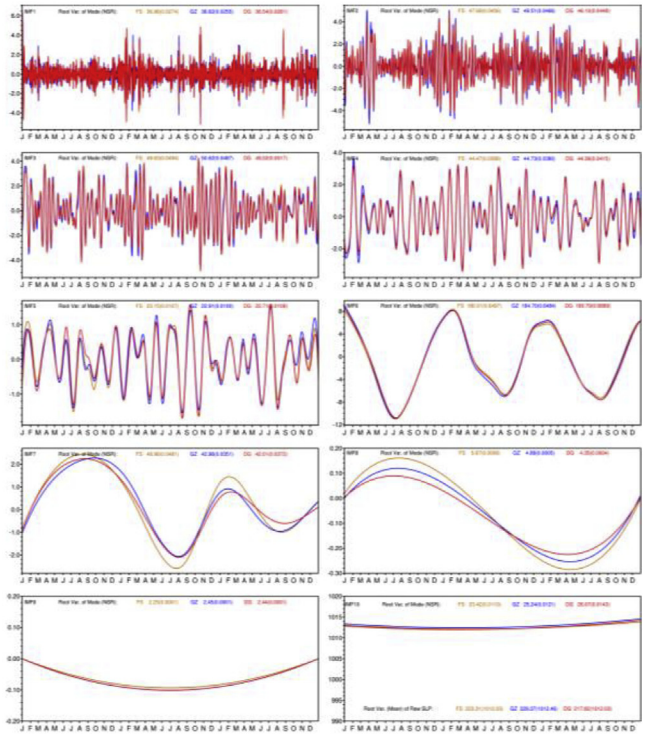

Fig. 6. (*continued*)

Table 1
FUL, WIN, and SUM sampling NSR_{IMF} of modes IMFs 1–7 of air quality (PM_{10}, $PM_{2.5}$, and O_3) and meteorological parameters (U, V, WS, RH, T, Q, and SP) in FGD during 2015 − 2017[a].

Sampling	Mode	PM_{10}	$PM_{2.5}$	O_3	U	V	WS	RH	T	Q	SP
FUL	IMF1	**0.14**	**0.15**	**0.16**	**0.21**	**0.16**	**0.31**	**0.15**	0.04	0.04	0.03
	IMF2	**0.13**	**0.12**	**0.11**	**0.14**	**0.13**	**0.20**	**0.13**	0.05	0.05	0.05
	IMF3	**0.15**	**0.13**	**0.16**	**0.13**	**0.12**	**0.19**	**0.13**	**0.06**	0.04	0.05
	IMF4	**0.10**	**0.12**	**0.08**	**0.08**	0.05	0.05	**0.12**	0.04	0.03	0.04
	IMF5	0.05	0.05	**0.07**	0.04	0.02	0.04	**0.08**	0.01	0.02	0.01
	IMF6	0.03	0.03	**0.07**	0.02	**0.07**	0.02	0.03	**0.49**	**0.25**	**0.65**
	IMF7	**0.19**	**0.22**	**0.11**	**0.12**	**0.18**	0.02	**0.08**	**0.06**	**0.15**	0.05
WIN	IMF1	**0.16**	**0.18**	**0.11**	**0.32**	**0.19**	**0.34**	**0.14**	0.04	0.04	0.03
	IMF2	**0.15**	**0.14**	**0.12**	**0.15**	**0.15**	**0.22**	**0.13**	0.05	**0.06**	**0.06**
	IMF3	**0.17**	**0.15**	**0.11**	**0.10**	**0.13**	**0.17**	**0.12**	**0.07**	**0.06**	**0.06**
	IMF4	**0.11**	**0.15**	**0.09**	0.04	0.05	0.05	**0.15**	0.04	0.04	0.04
	IMF5	0.05	0.05	**0.10**	0.03	0.02	0.04	**0.10**	0.01	0.02	0.01
	IMF6	0.02	0.02	**0.08**	0.03	0.04	0.01	0.03	**0.31**	**0.14**	**0.46**
	IMF7	**0.08**	**0.11**	**0.12**	**0.18**	**0.15**	0.02	**0.06**	0.05	**0.12**	0.02
SUM	IMF1	**0.11**	**0.10**	**0.20**	**0.16**	**0.13**	**0.27**	**0.16**	0.03	0.02	0.02
	IMF2	**0.08**	**0.07**	**0.10**	**0.14**	**0.11**	**0.18**	**0.12**	0.03	0.03	0.03
	IMF3	**0.10**	**0.11**	**0.20**	**0.15**	**0.11**	**0.20**	**0.14**	0.03	0.02	0.04
	IMF4	**0.08**	**0.08**	**0.07**	**0.10**	**0.06**	0.05	**0.08**	0.02	0.02	0.04
	IMF5	0.05	0.05	0.05	0.04	0.03	0.05	0.05	0.01	0.02	0.02
	IMF6	0.05	0.04	0.05	0.01	**0.12**	0.02	0.02	**0.79**	**0.40**	**0.87**
	IMF7	**0.46**	**0.45**	**0.09**	**0.09**	**0.23**	0.02	**0.12**	**0.07**	**0.19**	**0.09**

[a] Values larger than $\varphi^{-6} \cong 0.0557$ are in bold, where $\varphi = (1 + \sqrt{5})/2$.

correlation mechanisms between air quality and meteorology on individual scales.

3.3. Correlation mechanisms between PM and meteorology on lower frequency oscillations

As shown by the FUL sampling correlation coefficients of PM on mode IMF7 in Tables 2 and 3, PM in FGD has consistent significant negative correlations with U, V, T, RH, and Q on mode IMF7. Especially, $PM_{2.5}$ has quite good negative correlations with U (r = −0.60 ~ -0.84), V (r = −0.71 ~ -0.81), T (r = −0.63 ~ -0.80), RH (r = −0.65 ~ -0.86), and Q (r = −0.78 ~ -0.79). As a comparison, the apparent whole-scale correlation coefficients (in Table 5) of $PM_{2.5}$ at FS, GZ, and DG with U (r = −0.14, 0.03, and −0.18), V (r = −0.12, −0.03, −0.16), T (r = −0.11, −0.09, and −0.15), RH (r = −0.42, −0.38, and −0.48), Q (r = −0.35, −0.31, and −0.41) are either much less significant or mixing for interpretation.

As shown by IMF7 in Figs. 2 and 3, there are large positive (negative) anomalies of PM under cold dry northeasterly (warm moist southwesterly) anomalies during winter (summer) half year, which reflects the significant impact of EAM on PM. The significant PM-meteorology correlations on mode IMF7 can be clearly interpreted as follows. On the one hand, the ABL height is much lower during winter half year than during summer half year; on the other hand, more scavenging of PM is produced by summer monsoon precipitation. As for WIN (SUM) sampling, stronger cold northeasterly (warm

Table 2
FUL, WIN, and SUM sampling multi-scale correlation coefficients of PM_{10} with various meteorological parameters on modes IMFs 1–7 at FS[a].

Sampling	Mode	U	V	WS	RH	T	Q	SP
FUL	IMF1	0.07	0.19	**−0.30**	−0.02	**0.34**	0.27	−0.16
	IMF2	0.09	0.26	**−0.41**	−0.20	**0.43**	0.18	−0.19
	IMF3	−0.02	0.16	**−0.46**	**−0.48**	**0.51**	−0.02	−0.10
	IMF4	0.08	−0.13	**−0.51**	**−0.61**	0.27	**−0.43**	0.14
	IMF5	0.07	0.04	**−0.65**	**−0.30**	0.09	**−0.30**	0.27
	IMF6	−0.10	−0.27	−0.13	−0.22	−0.12	−0.20	0.16
	IMF7	**−0.71**	**−0.74**	−0.09	**−0.85**	**−0.68**	**−0.78**	**0.32**
WIN	IMF1	0.13	0.29	−0.30	0.03	**0.37**	0.33	−0.24
	IMF2	0.10	**0.39**	**−0.43**	−0.13	**0.41**	0.23	−0.24
	IMF3	0.01	**0.37**	**−0.51**	**−0.46**	**0.52**	0.08	−0.13
	IMF4	0.03	−0.03	**−0.54**	**−0.64**	0.29	**−0.42**	0.29
	IMF5	0.07	0.28	**−0.65**	−0.27	0.22	−0.24	0.29
	IMF6	0.29	0.02	0.25	−0.01	0.31	0.24	−0.28
	IMF7	**−0.70**	**−0.64**	**−0.54**	**−0.79**	−0.26	**−0.64**	0.09
SUM	IMF1	−0.03	−0.06	−0.31	−0.15	0.28	0.09	0.04
	IMF2	0.12	−0.10	**−0.40**	**−0.44**	**0.49**	−0.02	−0.01
	IMF3	−0.05	**−0.36**	**−0.44**	**−0.57**	**0.44**	**−0.35**	−0.04
	IMF4	0.16	−0.34	**−0.49**	**−0.50**	0.23	**−0.48**	−0.15
	IMF5	0.07	−0.29	**−0.66**	**−0.42**	−0.10	**−0.45**	0.28
	IMF6	**−0.44**	**−0.41**	**−0.43**	**−0.44**	−0.19	**−0.37**	0.24
	IMF7	**−0.52**	**−0.73**	**−0.42**	**−0.78**	**−0.68**	**−0.61**	0.29

[a] Coefficients with abstract value larger than 0.0993, 0.141, and 0.140 are significant on 0.001 level for FUL, WIN, and SUM, respectively; and coefficients with abstract value larger than 0.3 (0.35) are highlighted in bold for FUL (WIN & SUM).

Table 3
FUL, WIN, and SUM sampling multi-scale correlation coefficients of $PM_{2.5}$ with various meteorological parameters on modes IMFs 1–7 at FS[a].

Sampling	Mode	U	V	WS	RH	T	Q	SP
FUL	IMF1	0.05	0.20	−0.29	0.02	0.28	0.25	−0.14
	IMF2	0.09	0.19	**−0.41**	−0.18	**0.35**	0.13	−0.14
	IMF3	−0.04	0.12	**−0.49**	**−0.43**	**0.46**	0.00	−0.09
	IMF4	0.06	−0.10	**−0.46**	**−0.62**	0.24	**−0.43**	0.12
	IMF5	0.08	0.05	**−0.64**	**−0.27**	0.06	−0.25	0.25
	IMF6	−0.12	**−0.37**	−0.18	**−0.43**	−0.21	**−0.32**	0.28
	IMF7	**−0.77**	**−0.81**	−0.14	**−0.86**	**−0.71**	**−0.78**	**0.41**
WIN	IMF1	0.10	0.28	−0.29	0.07	0.29	0.30	−0.22
	IMF2	0.10	0.30	**−0.43**	−0.10	0.32	0.18	−0.18
	IMF3	0.02	0.34	**−0.54**	**−0.37**	**0.47**	0.10	−0.10
	IMF4	0.02	0.01	**−0.48**	**−0.66**	0.26	**−0.42**	0.27
	IMF5	0.11	0.34	**−0.64**	−0.22	0.18	−0.14	0.26
	IMF6	0.23	−0.19	0.05	−0.34	0.10	−0.03	−0.03
	IMF7	**−0.77**	**−0.72**	**−0.52**	**−0.75**	**−0.39**	**−0.67**	0.20
SUM	IMF1	−0.05	−0.03	−0.31	−0.10	0.25	0.12	0.04
	IMF2	0.11	−0.11	**−0.40**	**−0.41**	**0.46**	−0.04	−0.03
	IMF3	−0.11	**−0.38**	**−0.46**	**−0.56**	**0.43**	**−0.35**	−0.07
	IMF4	0.14	**−0.39**	**−0.49**	**−0.46**	0.19	**−0.46**	−0.19
	IMF5	0.07	−0.34	**−0.66**	**−0.40**	−0.15	**−0.49**	0.27
	IMF6	**−0.47**	**−0.43**	**−0.41**	**−0.48**	−0.17	**−0.42**	0.30
	IMF7	**−0.61**	**−0.83**	**−0.47**	**−0.86**	**−0.74**	**−0.69**	**0.43**

[a] Coefficients with abstract value larger than 0.0993, 0.141, and 0.140 are significant on 0.001 level for FUL, WIN, and SUM, respectively; and coefficients with abstract value larger than 0.3 (0.35) are highlighted in bold for FUL (WIN & SUM).

southwesterly) brings more polluted inland air (clean marine air) to GHMGBA, makes more accumulations (better dispersion) of PM, thus produces higher (lower) level of PM concentrations during winter (summer) half year. In addition, more precipitation is produced by stronger warm and moist southwesterly during summer half year. Therefore, the impact mechanisms of EAM on PM is the combined effects of vertical ventilation associated with T, horizontal dilution associated with U, V, and the large-scale PM gradient, as well as the wet deposition associated with RH and Q.

The correlations on mode IMF6 (80–90 days' oscillation) is a little complicated since several meteorological parameters like T, Q, and SP have frequency aliasing on modes IMF6 and IMF7. The apparent correlations with these parameters on mode IMF6 are not considered for the following discussion focusing on the 80–90 days' oscillation. As shown by the SUM sampling correlation coefficients in Tables 2 and 3, PM fractions in FGD generally have good negative correlations with U, V, WS, and RH on mode IMF 6 in summer half year. As shown by IMF6 in Figs. 2 and 3, large negative anomalies in PM are related to the large southerly and westerly anomalies (i.e., stronger summer monsoon) during the summer half year of 2015, which are mostly a response to the ENSO signal during the strong El Nino year 2015–2016, via scavenging mechanisms. As shown by the WIN sampling correlation coefficients in Tables 2 and 3, $PM_{2.5}$ in FGD has good negative (positive) correlations with V and RH (U) on mode IMF6 in winter half year. We also checked the correlations with $PM_{2.5\text{-}10}$ (the difference between PM_{10} and $PM_{2.5}$) in FGD (figure and table omitted) and found that

Table 4
FUL, WIN, and SUM sampling multi-scale correlation coefficients of O_3 with various meteorological parameters on modes IMFs 1–7 at FS[a].

Sampling	Mode	U	V	WS	RH	T	Q	SP
FUL	IMF1	−0.01	0.02	−0.26	**−0.41**	**0.39**	−0.10	0.08
	IMF2	−0.05	−0.03	**−0.35**	**−0.53**	**0.40**	−0.12	0.05
	IMF3	−0.15	−0.16	**−0.46**	**−0.67**	**0.40**	−0.25	−0.01
	IMF4	0.07	0.06	**−0.47**	**−0.65**	**0.48**	**−0.33**	0.17
	IMF5	−0.14	**−0.31**	**−0.46**	**−0.55**	0.28	**−0.47**	0.14
	IMF6	−0.23	−0.12	**−0.30**	0.00	**0.35**	0.23	−0.22
	IMF7	**0.60**	**0.36**	**−0.30**	**0.42**	**0.70**	**0.79**	−0.14
WIN	IMF1	0.01	0.02	−0.18	**−0.51**	**0.38**	−0.24	0.05
	IMF2	−0.11	0.07	−0.26	**−0.55**	0.29	−0.20	0.03
	IMF3	−0.01	0.17	**−0.36**	**−0.67**	**0.40**	−0.21	0.02
	IMF4	−0.03	0.22	**−0.53**	**−0.68**	**0.53**	−0.29	0.22
	IMF5	0.10	−0.15	−0.34	**−0.65**	**0.37**	**−0.56**	**0.39**
	IMF6	0.13	−0.01	−0.14	0.19	0.14	0.03	0.02
	IMF7	**0.66**	**0.42**	0.17	0.23	**0.87**	**0.74**	−0.21
SUM	IMF1	−0.02	0.01	**−0.35**	**−0.37**	**0.46**	0.01	0.11
	IMF2	−0.02	−0.15	**−0.45**	**−0.52**	**0.61**	−0.01	0.07
	IMF3	−0.20	**−0.46**	**−0.55**	**−0.74**	**0.58**	**−0.37**	−0.04
	IMF4	0.11	−0.14	**−0.42**	**−0.68**	**0.43**	**−0.41**	0.11
	IMF5	−0.32	**−0.51**	**−0.61**	**−0.36**	0.14	−0.31	−0.06
	IMF6	**−0.64**	**−0.48**	**−0.45**	**−0.51**	−0.06	**−0.40**	**0.38**
	IMF7	0.12	−0.31	−0.16	−0.29	−0.13	0.15	0.22

[a] Coefficients with abstract value larger than 0.0993, 0.141, and 0.140 are significant on 0.001 level for FUL, WIN, and SUM, respectively; and coefficients with abstract value larger than 0.3 (0.35) are highlighted in bold for FUL (WIN & SUM).

Table 5
FUL, WIN, and SUM sampling whole-scale correlation coefficients between PM_{10}, $PM_{2.5}$, and O_3, respectively, and various meteorological parameters at FS, GZ, and DG[a].

		FUL			WIN			SUM		
		PM_{10}	$PM_{2.5}$	O_3	PM_{10}	$PM_{2.5}$	O_3	PM_{10}	$PM_{2.5}$	O_3
FS	U	−0.12	−0.14	−0.01	−0.02	−0.04	0.02	−0.11	−0.13	−0.15
	V	−0.09	−0.12	−0.01	0.21	0.17	0.10	**−0.42**	**−0.44**	−0.34
	WS	**−0.44**	**−0.45**	**−0.45**	**−0.52**	**−0.53**	**−0.36**	**−0.45**	**−0.45**	**−0.56**
	T	−0.06	−0.11	**0.53**	0.33	0.24	**0.45**	0.12	0.11	**0.45**
	RH	**−0.45**	**−0.42**	**−0.49**	**−0.35**	−0.32	**−0.67**	**−0.53**	**−0.50**	**−0.63**
	Q	**−0.33**	**−0.35**	0.14	−0.02	−0.06	−0.18	**−0.46**	**−0.45**	−0.27
	SP	0.28	**0.30**	−0.24	−0.01	0.04	0.02	0.22	0.18	0.06
GZ	U	0.07	0.03	0.14	0.22	0.20	0.07	0.05	0.01	0.08
	V	0.01	−0.03	0.07	0.30	0.27	0.08	−0.28	−0.32	−0.15
	WS	**−0.43**	**−0.41**	**−0.37**	**−0.50**	**−0.49**	−0.26	**−0.44**	**−0.44**	**−0.49**
	T	−0.01	−0.09	**0.56**	**0.39**	0.30	**0.46**	0.22	0.18	**0.59**
	RH	**−0.43**	**−0.38**	**−0.54**	**−0.37**	−0.32	**−0.71**	**−0.51**	**−0.45**	**−0.63**
	Q	−0.28	**−0.31**	0.18	0.05	0.01	−0.19	**−0.35**	−0.33	−0.14
	SP	0.25	0.28	−0.25	−0.05	−0.01	0.07	0.22	0.16	0.00
DG	U	−0.14	−0.18	0.07	−0.04	−0.05	0.01	−0.09	−0.13	−0.02
	V	−0.11	−0.16	0.05	0.20	0.16	0.16	**−0.41**	**−0.44**	−0.26
	WS	**−0.45**	**−0.44**	**−0.48**	**−0.52**	**−0.52**	**−0.43**	**−0.46**	**−0.46**	**−0.56**
	T	−0.09	−0.15	**0.50**	0.28	0.24	**0.45**	0.17	0.11	**0.51**
	RH	**−0.49**	**−0.48**	**−0.48**	**−0.39**	**−0.36**	**−0.64**	**−0.53**	**−0.52**	**−0.61**
	Q	**−0.38**	**−0.41**	0.10	−0.10	−0.10	−0.17	**−0.44**	**−0.48**	−0.22
	SP	**0.30**	**0.34**	−0.18	0.03	0.06	0.03	0.21	0.22	0.06

[a] Coefficients with abstract value larger than 0.0993, 0.141, 0.140 are significant on 0.001 level for FUL, WIN, and SUM, respectively; and coefficients with abstract value larger than 0.3 (0.35) are highlighted in bold for FUL (WIN & SUM).

$PM_{2.5-10}$ has good positive correlations with U, V, WS, and RH on mode IMF6 in winter half year. It is obvious that the $PM_{2.5}$-RH correlation coefficients and the $PM_{2.5-10}$-RH correlation coefficients have different sign on mode IMF6 by WIN sampling. As shown by IMF6 in Fig. 6, there are large northerly anomalies during spring of 2015, winter of 2016, and autumn in 2017, which are probably impacted by the ENSO. Together with these negative V anomalies, there are large negative RH anomalies. Anomalies in U have sharp seasonal transition during spring of 2015 and autumn in 2017 and are generally out of phase with those V anomalies. WS has large anomalies in 2017 only. It seems that the positive correlations of $PM_{2.5-10}$ with U, V, WS, and RH on mode IMF6 in winter half year might be related to the variations in dust emission and advection which are dominantly impacted by WS. While the negative (positive) correlations of $PM_{2.5}$ with V and RH (U) on mode IMF 6 in winter half year might be due to scavenging of precipitation induced by the southeasterly anomalies during transition seasons.

3.4. Correlation mechanisms between PM and meteorology on higher frequency oscillations

As shown in Tables 2 and 3, PM has large positive (negative) correlations with V, T, and Q (WS and SP) on modes IMFs 1–3 and has large negative correlation with RH on mode IMF3 by WIN sampling. Under the impact of Nanling mountains (refer to the north part of Fig. 1 for the topography), there is usually a quasi-stationary front hovering over South China in winter half year. Before a new cold front comes, there is a period of several days when the FGD region is located at the warm sector of a quasi-stationary front. The front inversion suppresses the vertical dispersion, and the accumulation of high level of PM is accompanied with local warm advection, moist convergence, and updrafts at meso-low. Stagnation with low wind and high moisture (but no precipitation) also induces hygroscopic growth of PM. After a long period of seesaw battle, once a new cold front comes and the wet deposition is triggered, the PM level reduces rapidly. This is a very typical synoptic process in FGD (also in GHMGBA). The significant higher frequency energy reflects the close competitions of warm mass and cold mass. Modes IMFs 1 and 2 (i.e., 2–3 days' and 5–7 days' oscillations) in winter half year usually do not involve precipitation, since PM (except for $PM_{2.5-10}$ on mode IMF2 at DG) has quite good correlations with Q on modes IMFs 1 and 2 due to hygroscopic effect but poor and mixed correlations with RH. For example, the significant positive correlation with Q on mode IMF1 by WIN sampling is up to 0.29–0.33 for PM_{10}, 0.29–0.30 for $PM_{2.5}$, and 0.13–0.34 for $PM_{2.5-10}$, while the correlations with RH (either positive of negative) range only from 0.01 to 0.14. On the contrary, on mode IMF3 (i.e., quasi two weeks' oscillation), the negative correlations with RH by WIN sampling turn to be as good as 0.46–0.55 for PM_{10}, 0.37–0.49 for $PM_{2.5}$, and 0.48–0.55 for $PM_{2.5-10}$, which reflects the scavenging effect on PM from precipitation. Taking the above analyses together, the correlation mechanisms between PM and meteorology on modes IMFs 1–3 in winter half year are the combined effects of two sequential asymmetric processes: 1) a long no-precipitation stagnation period with alternating weak advantages of warm mass or cold mass when ventilation, dilution, and hygroscopic growth make effects; and 2) a short precipitation period associated with strong northerly, high RH, and cold T when ventilation, dilution, and wet deposition make effects. The accumulation of PM during the first period also contributes to the triggering of precipitation, which is a negative feedback mechanism.

As shown in Tables 2 and 3, PM has large negative (positive) correlations with WS, RH, and Q (T and SP) on modes IMFs 4 and 5 by WIN sampling. On the one hand, the dry downdraft anomalies accompanied with higher pressure and warm anomalies depresses the vertical dispersion of PM; on the other hand, the stagnation with lower wind favors the accumulations of PM. Therefore, the correlation mechanisms are the combined effects of enhanced dry downdraft suppression associated with SP, T, RH, and Q and the horizontal dispersion capability associated with WS.

As shown in Tables 2 and 3, PM has large negative (positive) correlations with WS and RH (T) on modes IMFs 1 and 2 by SUM sampling. On the one hand, the dry weather and subsidence inversion suppress the vertical ventilation of PM and the low wind situations reduce the horizontal dilution. On the other hand, warmer and drier surface is

related to more ground dust emission in summer half year. The fact that $PM_{2.5-10}$ has larger correlations with T and RH than $PM_{2.5}$ on modes IMFs 1 and 2 at FS and GZ supports this point, since ground dust is a major contribution to $PM_{2.5-10}$ in these two cities. $PM_{2.5-10}$ has smaller correlation with T than $PM_{2.5}$ at DG on modes IMFs 1 and 2 mostly because sea salt rather than ground dust contributes more to coarse PM at DG. The dry and hot weather under high pressure is typical in summer half year in FGD (also in GHMGBA), and the PM level is generally not high due to good ventilation and dilution. However, the persistent strong dry downdraft suppression induced by enhanced subtropical high or distant cyclones may make very high level of PM accumulations. The length of PM oscillation period depends on the duration of subsidence inversion which is usually related to duration of suppression and the moving speed of remote cyclones. Note that although PM fractions have good positive correlation with T on mode IMF2 (i.e., 5–7 days' oscillation) by SUM sampling: 0.49–0.52 for PM_{10}, 0.46–0.48 for $PM_{2.5}$, and 0.40–0.51 for $PM_{2.5-10}$, it is not the high surface temperature but the subsidence inversion that induces the PM accumulations.

Taken together, the correlation mechanisms of PM with WS, RH, and T on modes IMFs 1 and 2 in summer half year are the combined effects of dry downdraft suppression mostly driven by the subtropical high or remote cyclones, the enhanced upward surface flux of ground dust associated with low RH and hot T, and the horizontal dispersion capability associated with low WS.

As shown in Tables 2 and 3, PM has quite good negative correlations with V, WS, RH, and Q on modes IMFs 3–5 by SUM sampling. During summer half year, stronger southerly flow brings more moisture and produces more scavenging of PM by precipitation. The correlation mechanisms are the combined effects of the enhanced wet deposition associated with both RH and Q, dilution associated with WS, and the horizontal advection associated with V and regional scale PM gradient. The large positive correlation of PM with T on mode IMF3 is a coexisting phenomenon since precipitation in summer half year is usually accompanied with surface cooling.

3.5. Correlation mechanisms between O_3 and meteorology on lower frequency oscillation

As shown by the FUL WIN, and SUM sampling correlation coefficients of O_3 with various meteorological parameters on modes IMF7 in Table 4, O_3 has large positive correlation with U, V, T, RH and Q on mode IMF7 by FUL sampling, and the correlations are generally much more significant in winter half year. As shown by IMF7 in Figs. 4 and 6, there are large negative (positive) O_3 anomalies under the cold dry northeasterly (warm moist southwesterly) anomalies during winter (summer) half year, which reflects the significant impact of EAM on O_3. Basically, the shortwave radiation is much weaker and produces less O_3 during winter half year than during summer half year. In addition, the cold temperature in winter half year also depresses the production of volatile organic compounds which are important precursors of O_3. The main impact mechanisms of EAM on O_3 are the combined effects of seasonal oscillation of shortwave radiation associated with T and Q and the volatility variation associated with T. The positive correlations of O_3 with U, V, and RH on mode IMF7 are actually the coexisting phenomena. The reason for the less significant correlations by SUM sampling than by WIN sampling might be that the production of O_3 in summer half year is usually upper bounded by the availability of various precursors.

As shown by the FUL WIN, and SUM sampling correlation coefficients of O_3 on modes IMFs 5 and 6 in Table 4, O_3 have large negative correlations with U, V, WS, RH, and Q on modes IMFs 5 and 6 by SUM sampling. As shown by IMFs 5 and 6 in Figs. 4 and 6, large negative anomalies of O_3 during summer half year of 2015 are correlated with large positive anomalies in U and V (i.e., stronger summer monsoon). Basically, stronger (weaker) southwesterly brings more (less) moisture from ocean, induces more (less) cloud and lower (higher) level of shortwave radiation, and thus produce lower (higher) level of O_3. This reflects the impact of ENSO on O_3 during summer half year through modulations on oscillations of 40–60 days and 80–90 days, and the impact mechanisms are the combined effects of shortwave radiation variation in moist microphysics process associated with RH and Q and the local horizontal dilution associated with U, V, and WS.

3.6. Correlation mechanisms between O_3 and meteorology on higher frequency oscillations

As shown in Table 4, O_3 has large negative (positive) correlations with WS and RH (T) on modes IMFs 1 and 2 by SUM sampling and has large negative (positive) correlations with WS, RH and Q (T) on modes IMFs 1 and 2 by WIN sampling. These large correlations are represented well in the FUL sampling results. During both summer half year and winter half year, higher level of shortwave radiation associated with warmer and drier environments favors the production of more O_3, and lower WS induces the local accumulation of O_3. Therefore, on modes IMFs 1 and 2, the meteorological impact mechanisms on O_3 are generally consistent along the whole year, that is, the combined effects of shortwave radiation fluctuations associated with T, RH, and Q and the horizontal dispersion capability associated with WS.

As shown in Table 4, O_3 has large negative (positive) correlations with V, WS, RH, and Q (T) on mode IMF3 by SUM sampling and has large negative (positive) correlations with WS, RH, and Q (T and V) on mode IMF3 by WIN sampling. Basically, stronger southerly during summer half year brings more warm moist air, induces more warm clouds and less shortwave radiations, and produces less O_3, where the warm advection dominates over the radiation cooling. Weaker northerly during winter half year brings less cold dry air, induces less cold front clouds and more shortwave radiation, and produces more O_3. The impact mechanisms are the combined effects of shortwave radiation fluctuations associated with T, RH, and Q and the horizontal dispersion capability associated with WS and V.

As shown in Table 4, O_3 has large negative (positive) correlations with WS, RH and Q (T and SP) on mode IMFs 4 and 5 by WIN sampling. On the one hand, more shortwave radiation associated with high pressure and clear sky produces more O_3 in column; on the other hand, the subsidence accompanied with high pressure and dry warm air usually produces net downward transportation of O_3 and increases the level of surface O_3. Therefore, the impact mechanisms are the combined effects of shortwave radiation fluctuations, vertical transportation of O_3, and the horizontal dispersion capability associated with WS. Obviously, the less significant correlations between O_3 and meteorology on mode IMF4 by SUM sampling have similar mechanisms.

4. Conclusions and discussions

Philosophically, the response of air quality to weather and climate variabilities should be explored with a coherent multi-scale continuum of atmosphere in mind. In this paper, a multi-scale correlation analysis method is introduced to separate correlations on different scales for mechanism analysis by applying the correlation analysis on the intrinsic modes decomposed with the EEMD method. A combined analysis of the multi-scale correlations between air quality and meteorology in GHMGBA during 2015–2017 is performed. Some findings are summarized as follows:

(1) The air quality in GHMGBA has very significant high and low frequency oscillations that are typical oscillations in meteorology although the significance is variable.
(2) The apparent whole scale correlation coefficients cannot reflect real correlation details if the correlations on various frequency bands are very different even contrary.
(3) PM in GHMGBA has consistent significant negative correlations

with V, T, RH, and Q on seasonal oscillation, which reflects the significant impact of EAM. The impact mechanisms are the combined effects of vertical ventilation associated with T, horizontal dilution associated with U, V, and the large-scale PM gradient, as well as the wet deposition associated with RH and Q. PM generally has good negative correlations with U, V, WS, and RH on 80–90 days' oscillation in summer half year mostly via scavenging mechanisms. $PM_{2.5-10}$ generally has good positive correlations with U, V, WS, and RH on 80–90 days' oscillation in winter half year. $PM_{2.5}$ has good negative (positive) correlations with V and RH (U) on 80–90 days' oscillation in winter half year due to the scavenging of precipitation induced by southeasterly anomalies during transition seasons.

(4) PM in GHMGBA has large positive (negative) correlations with V, T, and Q (WS and SP) on oscillations of 2–3 days, 5–7 days, and quasi two weeks and has large negative correlation with RH on quasi two weeks' oscillation in winter half year. These correlations reflect the impact of the typical quasi-stationary front and cold front activities in winter half year. The correlation mechanisms are the combined effects of two sequential asymmetric processes: a long no-precipitation stagnation period with alternating weak advantages of warm mass or cold mass when ventilation, dilution, and hygroscopic growth make effects; and a short precipitation period associated with strong northerly, high RH, and cold T when ventilation, dilution, and wet deposition make effects. The accumulation of PM during the first period also contributes to the triggering of precipitation, which is a negative feedback mechanism. PM has large negative (positive) correlations with WS, RH, and Q (T and SP) on oscillations of 20–30 days and 40–60 days in winter half year. The correlation mechanisms are the combined effects of enhanced dry downdraft suppression associated with SP, T, RH, and Q and the horizontal dispersion capability associated with WS. PM has large negative (positive) correlations with WS and RH (T) on oscillations of 2–3 days and 5–7 days in summer half year. The correlation mechanisms are the combined effects of dry downdraft suppression mostly driven by the subtropical high or remote cyclones, the enhanced upward surface flux of ground dust associated with low RH and hot T, and the horizontal dispersion capability associated with low WS. PM has quite good negative correlations with V, WS, RH, and Q on oscillations of quasi two weeks, 20–30 days, and 40–60 days in summer half year. The correlation mechanisms are the combined effects of the enhanced wet deposition associated with both RH and Q, the dilution associated with WS, and the horizontal advection associated with V and regional scale PM gradient. The large positive correlation of PM with T on quasi two weeks' oscillation is a coexisting phenomenon.

(5) O_3 in GHMGBA has large positive correlation with U, V, T, RH and Q on seasonal oscillation, which reflects the significant impact of EAM on O_3. The main impact mechanisms are the combined effects of seasonal oscillation of shortwave radiation associated with T and Q and the volatility variation associated with T. The positive correlations of O_3 with U, V, and RH are actually the coexisting phenomena. The reason for the less significant correlations by SUM sampling than by WIN sampling might be that the production of O_3 in summer half year is usually upper bounded by the availability of various precursors. O_3 has large negative correlations with U, V, WS, RH, and Q on the inter-seasonal modes in summer half year. The impact mechanisms are the combined effects of shortwave radiation variation in moist microphysics process associated with RH and Q and the local horizontal dilution associated with U, V, and WS.

(6) O_3 in GHMGBA has large negative (positive) correlations with WS and RH (T) on oscillations of 2–3 days and 5–7 days in summer half year; and have large negative (positive) correlations with WS, RH and Q (T) on oscillations of 2–3 days and 5–7 days in winter half year. The meteorological impact mechanisms on O_3 are generally consistent along the whole year, that is, the combined effects of shortwave radiation fluctuations associated with T, RH, and Q and the horizontal dispersion capability associated with WS. O_3 has large negative (positive) correlations with V, WS, RH, and Q (T) on quasi two weeks' oscillation in summer half year, and has large negative (positive) correlations with WS, RH, and Q (T and V) on quasi two weeks' oscillation in winter half year. The impact mechanisms are the combined effects of shortwave radiation fluctuations associated with T, RH, and Q, and the horizontal dispersion capability associated with WS and V. O_3 has large negative (positive) correlations with WS, RH and Q (T and SP) on oscillations of 20–30 days and 40–60 days in winter half year. The impact mechanisms are the combined effects of shortwave radiation fluctuations, vertical transportation of O_3, and the horizontal dispersion capability associated with WS. The less significant correlations between O_3 and meteorology on oscillation of 40–60 days in summer half year have similar mechanisms.

Overall, an important contribution of this paper is that we introduced a multi-scale correlation analysis method that is useful to identify the respective main impact mechanisms of meteorology on air quality on different scales. Using this method, we can separate correlations on different scales without any other filtering or smoothing. The coherent multivariate multi-scale correlation analysis makes it possible to interpret correlation mechanisms on individual scale.

Multi-scale correlations were not considered even in a recent novel study by Shen et al. (2017), which was somehow as the extension and update of some previous studies (Tai et al., 2010, 2012a, 2012b). They regressed monthly mean $PM_{2.5}$ concentrations with both local meteorology and surrounding patterns diagnosed by singular value decomposition (SVD) algorithm and underscored the importance of evaluating the sensitivity of $PM_{2.5}$ to its key controlling meteorological variables in climate-chemistry models on multiple timescales before they are applied to project future air quality. Our results confirm the different scale sensitivity of PM to meteorology and alert careful extension of synoptic sensitivity for estimating the response of air quality to climate change projections.

In addition, the multi-scale correlation analysis method introduced in this paper might lead to a seamless multi-scale regression. Our future plan is to extend our work to build up a meteorology-based multi-scale multiple linear regression (MLR) statistic model for air quality study. Our idea should be not only good for day-to-day air quality forecasts but also useful for deriving more probability details of climate projection.

We do not consider the diurnal cycle in this paper, neither the relative abundance of PM components. More improvements can also be achieved in the future by considering some more relevant meteorological parameters, for example, the rainfall and radiation data, and on-site meteorological observations. Moreover, we do not include emissions in this study; further study on emission variabilities with relevant data available should benefit better understanding of air quality variabilities.

Acknowledgments

This work is supported by National Key R&D Program of China (No.2017YFC0209606, No.2016YFC0203305) and National Science Foundation Key Program of China (No.41630422).

References

Dawson, P.J., Adams, P.J., Pandis, S.N., 2007. Sensitivity of PM2.5 to climate in the Eastern US: a modeling case study. Atmos. Chem. Phys. 7, 4295–4309.

Dee, D.P., Uppala, S.M., Simmons, A.J., Berrisford, P., Poli, P., Kobayashi, S., Andrae, U., Balmaseda, M.A., Balsamo, G., Bauer, P., Bechtold, P., Beljaars, A.C.M., Berg, L.v.d., Bidlot, J., Bormann, N., Delsol, C., Dragani, R., Fuentes, M., Geer, A.J., Haimberger, L., Healy, S.B., Hersbach, H., Hólm, E.V., Isaksen, L., Kållberg, P., Köhler, M.,

Matricardi, M., McNally, A.P., Monge-Sanz, B.M., Morcrette, J.J., Park, B.K., Peubey, C., Rosnay, P.d., Tavolato, C., Thdrae, U., Balmaseda, M.A., Balsamo, G., 2011. Interim reanalysis: configuration and performance of the data assimilation system. Q. J. R. Meteorol. Soc. 137, 553–597.

Fan, S., Wang, B., Tesche, M., Engelmann, R., Althausen, A., Liu, J., Zhu, W., Fan, Q., Li, M., Ta, N., 2008. Meteorological conditions and structures of atmospheric boundary layer in October 2004 over Pearl River Delta area. Atmos. Environ. 42, 6174–6186.

Fan, S.J., Fan, Q., Yu, W., Luo, X.Y., Wang, B.M., Song, L.L., Leong, K.L., 2011. Atmospheric boundary layer characteristics over the Pearl River Delta, China, during the summer of 2006: measurement and model results. Atmos. Chem. Phys. 11, 6297–6310.

Fang, X., Kuo, Y.H., 2015. A new generic method for quantifying the scale predictability of the fractal atmosphere: applications to model verification. J. Atmos. Sci. 72, 1667–1688.

Galindo, N., Varea, M., Gil-Moltó, J., Yubero, E., Nicolás, J., 2010. The influence of meteorology on particulate matter concentrations at an urban mediterranean location. Water, Air, Soil Pollut. 215, 365–372.

Huang, N.E., Long, S.R., Shen, Z., 1996. The mechanism for frequency downshift in nonlinear wave evolution. In: Hutchinson, J.W., Wu, T.Y. (Eds.), Advances in Applied Mechanics. Elsevier, pp. 59–117C.

Huang, N.E., Shen, Z., Long, S.R., Wu, M.C., Shih, H.H., Zheng, Q., Yen, N.-C., Tung, C.C., Liu, H.H., 1998. The empirical mode decomposition and the Hilbert spectrum for nonlinear and non-stationary time series analysis. Proc. R. Soc. London, Ser. A: Math. Phys. Eng. Sci. 454, 903–995.

Jacobson, M.Z., 2001. Global direct radiative forcing due to multicomponent anthropogenic and natural aerosols. J. Geophys. Res.: Atmosphere 106, 1551–1568.

Ji, Z.P., Luo, S.B., Kuang, J.X., Luo, Q.H., Chen, M.S., Liang, G.X., 2006. Variation characteristics and prediction of air pollution in Guangzhou (in Chinese). J. Trop. Meteorol. 22, 574–581.

Leung, D.M., Tai, A.P.K., Mickley, L.J., Moch, J.M., van Donkelaar, A., Shen, L., Martin, R.V., 2017. Synoptic meteorological modes of variability for fine particulate matter (PM2.5) air quality in major metropolitan regions of China. Atmos. Chem. Phys. Discuss. 1–29.

Li, H., Wang, B., Fang, X., Zhu, W., Fan, Q., Liao, Z., Liu, J., Zhang, A., Fan, S., 2018. Combined effect of boundary layer recirculation factor and stable energy on local air quality in pearl river delta over southern China. J. Air Waste Manag. Assoc. 1–15.

Li, X., Ma, Y., Wang, Y., Liu, N., Hong, Y., 2017. Temporal and spatial analyses of particulate matter (PM 10 and PM 2.5) and its relationship with meteorological parameters over an urban city in northeast China. Atmos. Res. 198, 185–193.

Liao, Z., Sun, J., Yao, J., Liu, L., Li, H., Liu, J., Xie, J., Wu, D., Fan, S., 2018. Self-organized classification of boundary layer meteorology and associated characteristics of air quality in Beijing. Atmos. Chem. Phys. 18, 6771–6783.

Rosenfeld, D., Andreae, M.O., Asmi, A., Chin, M., de Leeuw, G., Donovan, D.P., Kahn, R., Kinne, S., Kivekäs, N., Kulmala, M., Lau, W., Schmidt, K.S., Suni, T., Wagner, T., Wild, M., Quaas, J., 2014. Global observations of aerosol-cloud-precipitation-climate interactions. Rev. Geophys. 52, 750–808.

Shen, L., Mickley, L.J., Murray, L.T., 2017. Influence of 2000–2050 climate change on particulate matter in the United States: results from a new statistical model. Atmos. Chem. Phys. 17, 4355–4367.

Tai, A.P.K., Mickley, L.J., Jacob, D.J., 2010. Correlations between fine particulate matter (PM2.5) and meteorological variables in the United States: implications for the sensitivity of PM2.5 to climate change. Atmos. Environ. 44, 3976–3984.

Tai, A.P.K., Mickley, L.J., Jacob, D.J., 2012a. Impact of 2000–2050 climate change on fine particulate matter (PM2.5) air quality inferred from a multi-model analysis of meteorological modes. Atmos. Chem. Phys. 12, 11329–11337.

Tai, A.P.K., Mickley, L.J., Jacob, D.J., Leibensperger, E.M., Zhang, L., Fisher, J.A., Pye, H.O.T., 2012b. Meteorological modes of variability for fine particulate matter (PM2.5) air quality in the United States: implications for PM2.5 sensitivity to climate change. Atmos. Chem. Phys. 12, 3131–3145.

Wu, D., Liao, B.T., Chen, H.Z., Wu, C., 2014a. Advances in studies of haze weather over peral river delta (in Chinese). Climatic Environ. Res. 19, 248–264.

Wu, M., Wu, D., Fan, Q., Wang, B.M., Li, H.W., Fan, S.J., 2013. Observational studies of the meteorological characteristics associated with poor air quality over the Pearl River Delta in China. Atmos. Chem. Phys. 13, 10755–10766.

Wu, M., Wu, D., Fan, S.J., Chen, H.Z., Pan, H.M., 2014b. Research Progress in the study of air pollution and atmospheric boundary layer over the pearl river delta city cluster (in Chinese). Adv. Meteorol. Sci. Technol. 22–28.

Wu, Z., Feng, J., Qiao, F., Tan, Z.M., 2016. Fast multidimensional ensemble empirical mode decomposition for the analysis of big spatio-temporal datasets. Philos. Trans. A Math. Phys. Eng. Sci. 374, 20150197.

Wu, Z.H., Huang, N.E., 2009. Ensemble empirical mode decomposition: a noise-assisted data analysis method. Adv. Adapt. Data Anal. 01, 1–41.

Yadav, R., Beig, G., Jaaffrey, S.N.A., 2014. The linkages of anthropogenic emissions and meteorology in the rapid increase of particulate matter at a foothill city in the Arawali range of India. Atmos. Environ. 85, 147–151.

Zhang, H., Wang, Y., Hu, J., Ying, Q., Hu, X.M., 2015. Relationships between meteorological parameters and criteria air pollutants in three megacities in China. Environ. Res. 140, 242–254.

Zhang, J.P., Zhu, T., Zhang, Q.H., Li, C.C., Shu, H.L., Ying, Y., Dai, Z.P., Wang, X., Liu, X.Y., Liang, A.M., Shen, H.X., Yi, B.Q., 2012. The impact of circulation patterns on regional transport pathways and air quality over Beijing and its surroundings. Atmos. Chem. Phys. 12, 5031–5053.

Zhang, Y., Ding, A., Mao, H., Nie, W., Zhou, D., Liu, L., Huang, X., Fu, C., 2016. Impact of synoptic weather patterns and inter-decadal climate variability on air quality in the North China Plain during 1980–2013. Atmos. Environ. 124, 119–128.

Zhou, D., Ding, A., Mao, H., Fu, C., Wang, T., Chan, L.Y., Ding, K., Zhang, Y., Liu, J., Lu, A., Hao, N., 2013. Impacts of the East Asian monsoon on lower tropospheric ozone over coastal South China. Environ. Res. Lett. 8, 044011.